Electrochemistry
The Electrochemical Society of Japan
Received: December 2, 2022
Accepted: December 20, 2022
Published online: December 23, 2022
Issued: January 25, 2023
https://doi.org/10.5796/electrochemistry.22-00126
Note
Electrochemistry, 91(1), 017003 (2023)

Electrochemical Investigation of Spherical Hard Carbon Negative Electrodes for Sodium Secondary Batteries

Shubham KAUSHIK, Kazuhiko MATSUMOTO,§ and Rika HAGIWARA*,§§

Graduate School of Energy Science, Kyoto University, Yoshida-honmachi, Sakyo-ku, Kyoto 606-8501, Japan

** Corresponding author: hagiwara@energy.kyoto-u.ac.jp, Tel: +81-75-753-5822, Fax: +81-75-753-5906*

ABSTRACT

Hard carbon (HC) is receiving widespread attention as a negative electrode material for sodium secondary batteries. In this study, spherical HC with three different diameters (1 µm, 1.5 µm, and 5 µm) are investigated using ionic liquid (IL) and organic electrolytes. The HC with a diameter of 5 µm demonstrated the best performance with IL at 90 °C (capacities of 327 mAh g^{-1} at 20 mA g^{-1} and 77 mAh g^{-1} at 2000 mA g^{-1} and initial Coulombic efficiency of 78.9 %). The HCs showed stable cycling in ILs as compared to the organic electrolytes in the first few cycles.

Keywords : Spherical Hard Carbon, Negative Electrode, Ionic Liquid, Intermediate Temperature

1. Introduction

During the last few decades, lithium-ion batteries (LIBs) have been widely accepted in applications for portable devices and electric vehicles owing to their high energy and power densities and long lifespan.[1–3] However, the limited amount of Li resources in the earth crust and seawater has motivated researchers to study post Li chemistries such as Na-ion batteries (SIBs).[4] Other major issues with the current LIBs are the flammability and volatility of the organic solvents used in the electrolyte, which poses safety concerns at elevated temperatures.[5–7] Ionic liquids (ILs) offer low flammability, negligible volatility, wide electrochemical window, and high ionic conductivity which make them promising electrolyte candidates to construct safe and high performance LIBs as well as post LIBs.[8,9] SIBs using IL electrolytes have been well studied and this system demonstrated long cycleability and high rate capabilities at wide temperature range.[10–16]

In the case of LIBs, graphitized carbon materials are considered as the negative electrode candidates owing to their low potential, environmentally benign nature, high stability in cycling, and low cost.[17] Unfortunately, graphite cannot be utilized in Na systems because of the thermodynamic instability of the sodium graphite intercalation compound.[18,19] Therefore, alternative negative electrode materials such as phosphorous,[20] phosphides,[21–23] and carbonaceous materials[24,25] such as soft carbon, amorphous carbon materials, and carbon nanostructures have been explored. For instance, hard carbon (HC) is intensively investigated as a negative electrode material for SIBs.[26–28] It consists of turbostratic domain and tunable nanopores which can also provide active sites for Na storage. In 2011, a comprehensive study conducted on the investigation of electrochemical Na^+ insertion behavior in commercially available HC revealed a characteristic charge-discharge profile consisting of sloping and plateau profiles at high (1.2–0.1 V) and low voltage (0.1–0 V), respectively, providing discharge capacities of 220 mAh g^{-1}. Furthermore, an HC/$NaNi_{0.5}Mn_{0.5}O_2$ full cell displayed a high capacity of 200 mAh g^{-1} (on HC basis) and an operating voltage of 3 V at room temperature.[29] In another study, HC prepared by pyrolysis of sugar exhibited a high capacity of ~300 mAh g^{-1} at 0.1 C (1 C = 1 Na^+ in 1 h) in 1 mol dm^{-3} $NaClO_4$-EC:PC (EC = ethylene carbonate and PC = propylene carbonate).[30] However, the addition of fluoroethylene carbonate (FEC) additive severely degraded the cycleability owing to the increased polarization. Another comprehensive study reported the effect of HC porosity on the reversible capacity. The porosity was controlled by adjusting the pyrolysis temperature, providing a high reversible capacity of 335 mAh g^{-1} with a BET surface area of 24.8 m^2 g^{-1} (cf. 199 mAh g^{-1} with a BET surface area of 265.8 m^2 g^{-1}).[31] HC in spherical morphology is a popular choice for electrochemical investigation owing to the uniform Na^+ ion flux across the particle surface.[32,33] HC microspheres prepared by microwave synthesis using sucrose as the starting material provided a high initial discharge capacity of 385 mAh g^{-1} at 30 mA g^{-1}.[34] However, there is no systematic investigation of particle size effect of spherical HC on the electrochemical performance in SIBs. Although various organic electrolytes were employed in SIBs,[35,36] IL electrolytes have also been employed for HC negative electrode materials in SIBs. In a preliminary study, HC with the Na[FSA]–[C_3C_1pyrr][FSA] (FSA^- = bis(fluorosulfonyl)amide and $C_3C_1pyrr^+$ = *N*-methyl-*N*-propylpyrrolidinium) IL showed a high rate capability at 90 °C, exhibiting 211 mAh g^{-1} at 1000 mA g^{-1}.[37] As an extension of this work, the electrochemical performance of HC with the Na[FSA]–[C_3C_1pyrr][FSA] IL was investigated in a wide temperature range from −10 to 90 °C.[38] A high capacity retention of 84 % was observed for 500 cycles at 90 °C. However, the limited reversible capacity of 25 mAh g^{-1} was observed at 25 °C. According to the aforementioned studies, the particle size and pore size of HC as well as the structures of electrolytes are the key factors to determine the reversible capacity, side reactions, and rate capability in Na secondary batteries. Therefore, it is of great importance to investigate these factors to systematically design HC for practical applications.

In this study, spherical HC of three different diameters (HC-1 (diameter: 1 µm and surface area: 17 m^2 g^{-1}), HC-1.5 (diameter: 1.5 µm diameter, surface area: 17 m^2 g^{-1}), and HC-5 (diameter: 5 µm

§ECSJ Active Member
§§ECSJ Fellow
S. Kaushik orcid.org/0000-0002-2534-2897
K. Matsumoto orcid.org/0000-0002-0770-9210
R. Hagiwara orcid.org/0000-0002-7234-3980

and surface area: $6\,m^2\,g^{-1}$) were investigated with the Na[FSA]–$[C_3C_1pyrr][FSA]$ IL at 25 and 90 °C for SIBs. A series of control experiments were performed with organic electrolytes with $[FSA]^-$ and $[PF_6]^-$ anions in the presence/absence of FEC additive.

2. Experimental

Spherical HCs HC-1, HC-1.5, and HC-5 were provided by Air Water Bellpearl Inc. The XRD patterns of the samples were obtained from a Rigaku SmartLab diffractometer (CuKα (1.5418 Å), 40 kV–30 mA). Particle size and morphology were analyzed by scanning electron microscopy (SEM, Hitachi SU-8020). The slurry of the HC electrode was prepared by mixing HC, acetylene black (AB), and polyamideimide binder in the ratio of 90 : 5 : 5 wt% with *N*-methyl-2-pyrrolidone (Wako Pure Chemical Industries, purity >99 %) maintaining solid/liquid ratio of 4/6 w/w. The resulting slurry was coated on Al foil using a compact sheet coating machine (Hohsen Corp.) with a desired electrode thickness of 40 µm and subsequently dried in a vacuum oven at 60 °C overnight and in a vacuum line at 120 °C for 10 h. The electrodes were cut into 10 mm discs with an average HC mass loading of $2\,mg\,cm^{-2}$. Sodium metal (Aldrich, purity 99.9 %) for counter electrodes was cut into 13 mm discs and pressed on Al discs (16 mm). The Na[FSA] (Mitsubishi Materials Electronic Chemicals Co., Ltd., purity >99 %) and $[C_3C_1pyrr][FSA]$ (Kanto Chemical Co., Inc., purity >99.9 %) salts were dried under vacuum at 90 °C overnight before mixing in the 2 : 8 mol ratio. The IL electrolyte was vacuum-impregnated into a separator (Whatman, GF-A, 260 mm in thickness and 16 mm in diameter) for 10 h before assembling coin cells. For control experiments, organic electrolytes were prepared by dissolving $1\,mol\,dm^{-3}$ of Na[FSA] (Org_{FSA}) or $Na[PF_6]$ (Org_{PF6}) into EC : DMC (DMC = dimethyl carbonate) (1 : 1 v/v) (Kishida Chemicals). In order to examine the effects of the additive, 3 wt% FEC (Wako Pure Chemical Industries) was added to the freshly prepared Org_{FSA} and Org_{PF6}.

The electrochemical behavior was measured using an HJ1001SD8 charge–discharge test device (Hokuto Denko). A two-electrode 2032-type coin-cell was assembled in a glove box (Miwa Manufacturing Co., Ltd., DBO-2LKH-HNBR) filled with dry and deoxygenated Ar gas. The operating temperature was maintained at 25 and 90 °C in the case of the IL electrolyte and 25 °C in the case of organic electrolytes.

3. Results and Discussion

The morphological and structural characterizations of the HCs were performed using SEM and XRD as shown in Fig. 1. Figures 1a–1c shows the SEM images of HC-1, HC-1.5 and HC-5, respectively. The spherical morphology of the HCs can be clearly observed and the average particle size is close to the expected value. The surface of HC-1 and HC-5 particles is apparently smooth, whereas surface roughness is observed for HC-1.5 (Fig. 1b). Figure 1d shows the XRD patterns of HC-1, HC-1.5, and HC-5. Each sample displays the broad 002 and 10 diffraction peaks ascribed to a hexagonal lattice of graphite at 22.6 and 42.6°, confirming the disordered HC structure with low crystallinity.

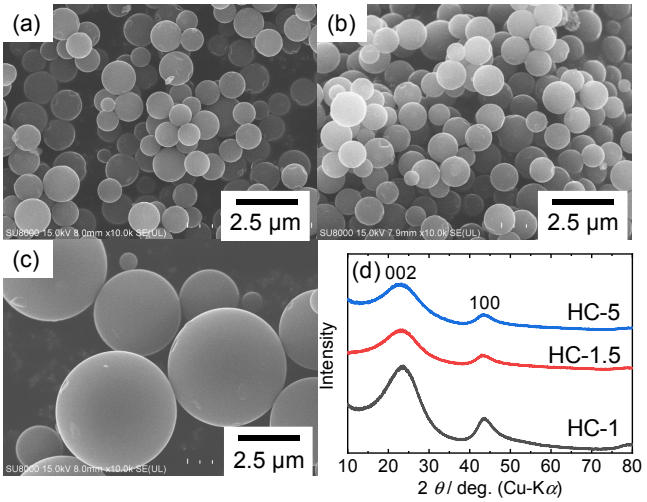

Figure 1. SEM images of (a) HC-1, (b) HC-1.5, and (c) HC-5. (d) XRD patterns of HC-1, HC-1.5, and HC-5.

Figures 2a–2c shows the galvanostatic charge-discharge curves of the first two cycles for HC-1, HC-1.5, and HC-5, respectively, using the IL electrolyte at 25 and 90 °C (current density of $20\,mA\,g^{-1}$). According to previous works,[12] operation at intermediate temperatures including 90 °C effectively enhances battery performance by using ubiquitous waste heat as confirmed in previous works. The typical sloping behavior in the high voltage region and plateau behavior in the low voltage region are observed in all the cases, corresponding to Na^+ insertion into the turbostratic graphitic domain and the nanopores, respectively. At 25 °C, HC-1, HC-1.5, and HC-5 exhibit discharge capacities of 207, 275 and $235\,mAh\,g^{-1}$ with initial Coulombic efficiencies of 80.8, 80.4, and 86.1 %, respectively. The enhanced discharge capacity for HC-1.5 can be attributed to the additional active sites, but the increased surface activity also causes the irreversible capacity of HC-1.5 (similar to HC-1 despite the larger diameter). At 90 °C, HC-5 displays the superior initial discharge capacity of $332\,mAh\,g^{-1}$ to

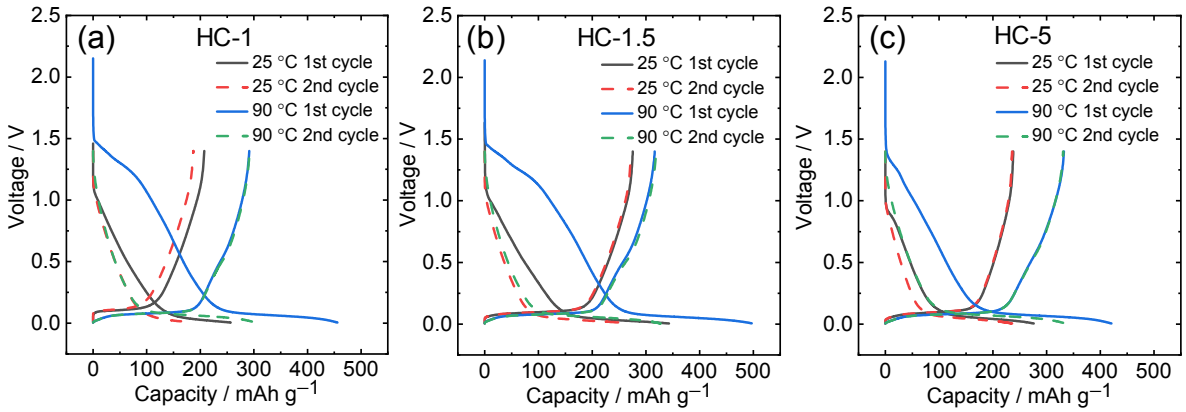

Figure 2. Galvanostatic charge-discharge curves of the Na/HC cells ((a) HC-1, (b) HC-1.5, and (c) HC-5) at 25 and 90 °C using the IL electrolyte for the first and second cycles. Current density = $20\,mA\,g^{-1}$ and cut-off voltage = 0.005–1.4 V. The capacity was calculated based on the weight of HC in the electrode.

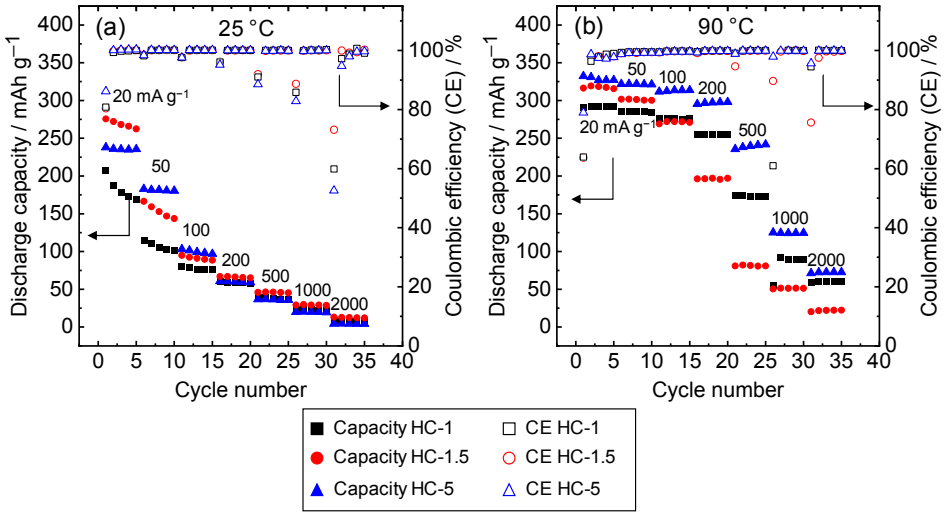

Figure 3. Rate capability of the Na/HC cells (HC = HC-1, HC-1.5, and HC-5) using the IL electrolyte at (a) 25 °C and (b) 90 °C. Current density = 20–2000 mA g^{-1} and cut-off voltage = 0.005–1.4 V. CE = Coulombic efficiency.

Table 1. Summary of the discharge capacities and initial Coulombic efficiencies for HC-1, HC-1.5, and HC-5 using the IL electrolyte at 25 and 90 °C.[a]

Temperature (°C)	Discharge capacity (mAh g^{-1})												Initial Coulombic efficiency (%)		
	HC-1 Current density (mA g^{-1})				HC-1.5 Current density (mA g^{-1})				HC-5 Current density (mA g^{-1})				HC-1	HC-1.5	HC-5
	20	100	500	2000	20	100	500	2000	20	100	500	2000			
25	169	76	36	6.9	262	89	45	13	235	97	36	4.2	80.8	80.4	86.1
90	291	275	177	61	317	271	81	22	327	313	241	77	63.9	63.7	78.9

[a]The discharge capacity reported in this table corresponds to the fifth cycle of each current in the rate capability test in Fig. 3.

291 and 317 mAh g^{-1} for HC-1 and HC-1.5, respectively. In terms of initial Coulombic efficiency, HC-5 demonstrates the highest value of 78.9 %, whereas HC-1 and HC-1.5 exhibit 63.9 and 63.7 %, respectively.

Figure 3 shows the rate capabilities of HC-1, HC-1.5, and HC-5 at 25 and 90 °C using the IL electrolyte. The current density was varied in the 20–2000 mA g^{-1} range and the cut-off voltage was set to 0.005–1.4 V. At 25 °C, HC-1.5 displays the highest capacity at 20 mA g^{-1} (275 mAh g^{-1}) among the HCs as shown in Fig. 3a. However, at 50 mA g^{-1}, the discharge capacity of HC-5 (180 mAh g^{-1}) surpasses that of HC-1.5 (143 mAh g^{-1}). One possible reason for this behavior is the large porosity of the HC-5 electrode because the composite electrode of large particles usually has more space inside, which enables facile Na^+ ion transport. At higher rates, the capacities are similar to each other and decreased gradually with increasing the rate, although the Coulombic efficiencies were maintained close to 100 %. Regardless of the size of HC, the rate capability at 90 °C significantly improves compared to that at 25 °C (Fig. 3b). HC-5 demonstrates the highest capacities in the entire current density range. Although HC-1.5 shows higher capacities than those of HC-1 in the current density range from 20 to 100 mA g^{-1}, it flips in the higher rates. Table 1 summarizes the reversible discharge capacities in the fifth cycle at each rate and initial Coulombic efficiencies at 25 and 90 °C. Overall, it can be inferred that particle size, porosity, and operation temperature affect the discharge capacity, irreversible capacity, and rate capability. It is possible that a larger particle size, with a smaller surface area, suppresses the electrolyte decomposition at 90 °C, resulting in formation of effective solid electrolyte interphase (SEI) and allowing facile Na^+ migration through the electrode/electrolyte interface.[39]

As a control experiment, the charge-discharge behavior of the HCs was analyzed in organic electrolytes Org_{FSA} and Org_{PF6} with and without FEC additive as shown in Fig. 4. In the case of Org_{FSA} (Figs. 4a–4c), the discharge capacity in the first cycle increases with increasing particle size, displaying 206, 253, and 292 mAh g^{-1} for HC-1, HC-1.5, and HC-5, respectively. A similar trend is observed for the initial Coulombic efficiencies (70.9, 77.1, and 81.5 % in HC-1, HC-1.5, and HC-5, respectively). In the fifth cycle, HC-5 retains a capacity of 244 mAh g^{-1}, whereas severe capacity fading is observed for HC-1 and HC-1.5. In the case of Org_{PF6}, the discharge capacity and Coulombic efficiency are highly improved as compared to Org_{FSA} in HC-1 and HC-1.5 exhibiting 284 and 290 mAh g^{-1} and 81.8 and 80.4 % in the first cycle, respectively. HC-5 with Org_{PF6} displayed a similar capacity and a Coulombic efficiency of 289 mAh g^{-1} and 81.7 % to those with Org_{FSA}. In the fifth cycle, the capacity and Coulombic efficiency are significantly decreased, suggesting instability of charge-discharge behavior in organic electrolytes. According to the charge-discharge curves, the addition of FEC additive increases polarization in any case probably due to the formation of SEI with high resistance. From these results, it is clearly observed that HCs with ILs provided superior cycle stability than that in HCs with organic electrolytes.

4. Conclusion

In the present study, the electrochemical behavior of spherical HCs with three different sizes was systematically investigated at 25 and 90 °C as negative electrode materials for SIBs using an IL electrolyte. At 25 °C, HC-1.5 exhibits the highest discharge capacity of 262 mAh g^{-1} at 20 mA g^{-1} among the HCs with the initial

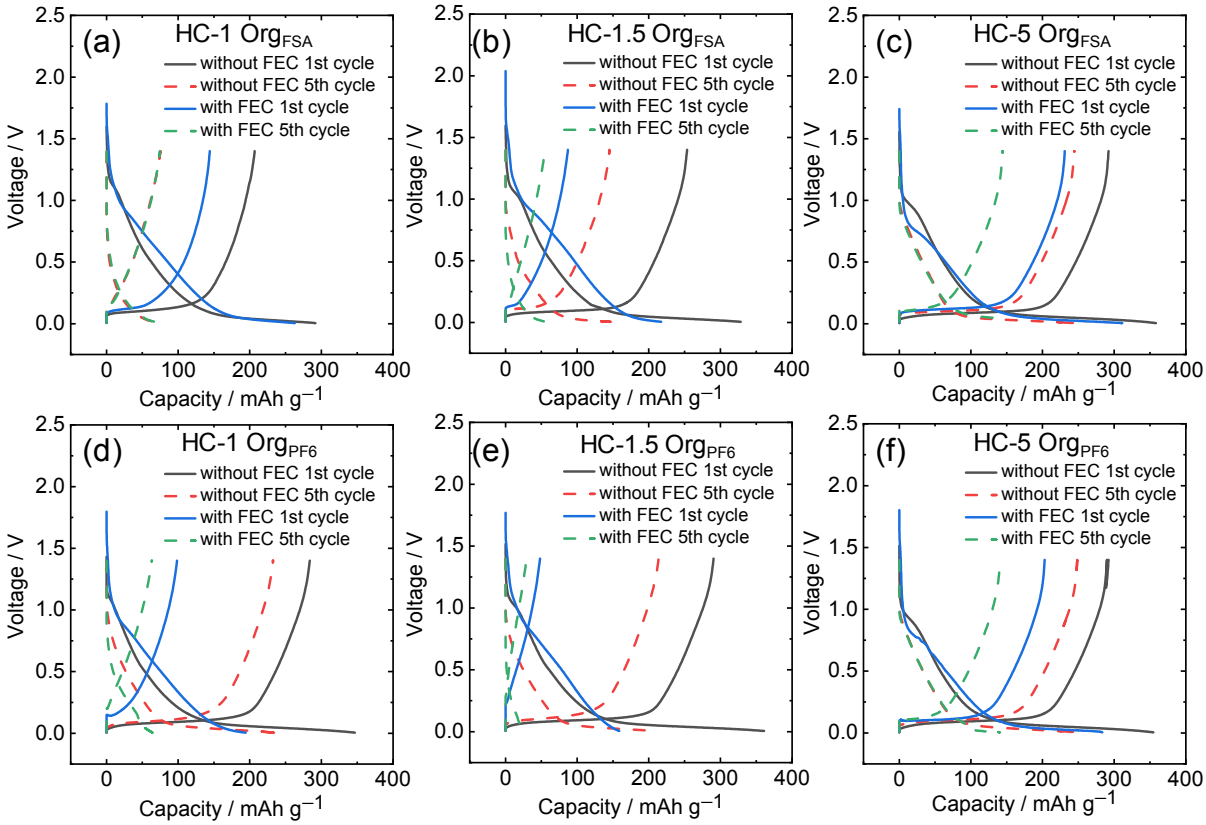

Figure 4. Galvanostatic charge-discharge curves of the Na/HC cells using Org$_{FSA}$ electrolyte with and without FEC additive ((a) HC-1, (b) HC-1.5, and (c) HC-5) and using Org$_{PF6}$ electrolyte with and without FEC additive ((d) HC-1, (e) HC-1.5, and (f) HC-5)) at 25 °C for the first and second cycles. Current density = 20 mA g^{-1} and cut-off voltage = 0.005–1.4 V.

Coulombic efficiency of 80.4 %. This enhanced capacity could be attributed to the presence of active sites on the particle surface. Similar capacities were observed regardless of particle size at high rates. At 90 °C, HC-5 demonstrated superior discharge capacity and rate capability (327 and 77 mAh g^{-1} at 20 and 2000 mA g^{-1}, respectively). In the cases of organic electrolytes, higher capacities and higher Coulombic efficiencies were observed with Org$_{PF6}$ than with Org$_{FSA}$, and the introduction of the FEC additive degraded the performance by increasing the polarization in both cases.

Acknowledgments

Hard carbon materials were supplied by Air Water Bellpearl Inc.

CRediT Authorship Contribution Statement

Shubham Kaushik: Data curation (Lead), Investigation (Lead), Methodology (Lead), Writing – original draft (Lead)
Kazuhiko Matsumoto: Methodology (Supporting), Project administration (Supporting), Supervision (Supporting), Writing – review & editing (Supporting)
Rika Hagiwara: Supervision (Lead), Validation (Lead), Writing – review & editing (Lead)

Conflict of Interest

The authors declare no conflict of interest in the manuscript.

References

1. A. Manthiram, *Nat. Commun.*, **11**, 1550 (2020).
2. X. Zeng, M. Li, D. Abd El-Hady, W. Alshitari, A. S. Al-Bogami, J. Lu, and K. Amine, *Adv. Energy Mater.*, **9**, 1900161 (2019).
3. R. Marom, S. F. Amalraj, N. Leifer, D. Jacob, and D. Aurbach, *J. Mater. Chem.*, **21**, 9938 (2011).
4. S. R. Taylor, *Geochim. Cosmochim. Acta*, **28**, 1273 (1964).
5. C. Arbizzani, G. Gabrielli, and M. Mastragostino, *J. Power Sources*, **196**, 4801 (2011).
6. A. Guerfi, M. Dontigny, P. Charest, M. Petitclerc, M. Lagacé, A. Vijh, and K. Zaghib, *J. Power Sources*, **195**, 845 (2010).
7. T. Tsujikawa, K. Yabuta, T. Matsushita, T. Matsushima, K. Hayashi, and M. Arakawa, *J. Power Sources*, **189**, 429 (2009).
8. J.-K. Kim, A. Matic, J.-H. Ahn, and P. Jacobsson, *J. Power Sources*, **195**, 7639 (2010).
9. J. Kalhoff, G. G. Eshetu, D. Bresser, and S. Passerini, *ChemSusChem*, **8**, 2154 (2015).
10. K. Matsumoto, Y. Okamoto, T. Nohira, and R. Hagiwara, *J. Phys. Chem. C*, **119**, 7648 (2015).
11. S. A. Mohd Noor, P. C. Howlett, D. R. MacFarlane, and M. Forsyth, *Electrochim. Acta*, **114**, 766 (2013).
12. K. Matsumoto, J. Hwang, S. Kaushik, C.-Y. Chen, and R. Hagiwara, *Energy Environ. Sci.*, **12**, 3247 (2019).
13. I. Hasa, S. Passerini, and J. Hassoun, *J. Power Sources*, **303**, 203 (2016).
14. J. Hwang, K. Matsumoto, and R. Hagiwara, *Adv. Sustain. Syst.*, **2**, 1700171 (2018).
15. H. Usui, Y. Domi, M. Shimizu, A. Imoto, K. Yamaguchi, and H. Sakaguchi, *J. Power Sources*, **329**, 428 (2016).
16. N. Yabuuchi, K. Kubota, M. Dahbi, and S. Komaba, *Chem. Rev.*, **114**, 11636 (2014).
17. T. Ohzuku, Y. Iwakoshi, and K. Sawai, *J. Electrochem. Soc.*, **140**, 2490 (1993).
18. H. Kim, J. Hong, G. Yoon, H. Kim, K.-Y. Park, M.-S. Park, W.-S. Yoon, and K. Kang, *Energy Environ. Sci.*, **8**, 2963 (2015).
19. O. Lenchuk, P. Adelhelm, and D. Mollenhauer, *Phys. Chem. Chem. Phys.*, **21**, 19378 (2019).
20. M. Dahbi, M. Fukunishi, T. Horiba, N. Yabuuchi, S. Yasuno, and S. Komaba, *J. Power Sources*, **363**, 404 (2017).
21. H. Usui, Y. Domi, R. Yamagami, K. Fujiwara, H. Nishida, and H. Sakaguchi, *ACS Appl. Energy Mater.*, **1**, 306 (2018).
22. H. Usui, Y. Domi, R. Yamagami, and H. Sakaguchi, *Green Energy Environ.*, **4**, 121 (2019).
23. H. Usui, Y. Domi, K. Fujiwara, M. Shimizu, T. Yamamoto, T. Nohira, R. Hagiwara, and H. Sakaguchi, *ACS Energy Lett.*, **2**, 1139 (2017).
24. H. Zhang, Y. Huang, H. Ming, G. Cao, W. Zhang, J. Ming, and R. Chen, *J. Mater. Chem. A*, **8**, 1604 (2020).

25. B. Cao, H. Liu, B. Xu, Y. Lei, X. Chen, and H. Song, *J. Mater. Chem. A*, **4**, 6472 (2016).
26. B. Xiao, T. Rojo, and X. Li, *ChemSusChem*, **12**, 133 (2019).
27. K. Wang, Y. Jin, S. Sun, Y. Huang, J. Peng, J. Luo, Q. Zhang, Y. Qiu, C. Fang, and J. Han, *ACS Omega*, **2**, 1687 (2017).
28. T. Yamamoto, T. Yamaguchi, T. Nohira, R. Hagiwara, A. Fukunaga, S. Sakai, and K. Nitta, *Electrochemistry*, **85**, 391 (2017).
29. S. Komaba, W. Murata, T. Ishikawa, N. Yabuuchi, T. Ozeki, T. Nakayama, A. Ogata, K. Gotoh, and K. Fujiwara, *Adv. Funct. Mater.*, **21**, 3859 (2011).
30. A. Ponrouch, A. R. Goñi, and M. R. Palacín, *Electrochem. Commun.*, **27**, 85 (2013).
31. C. Bommier, W. Luo, W.-Y. Gao, A. Greaney, S. Ma, and X. Ji, *Carbon*, **76**, 165 (2014).
32. L. Yang, M. Hu, Q. Lv, H. Zhang, W. Yang, and R. Lv, *Carbon*, **163**, 288 (2020).
33. H. D. Asfaw, C. W. Tai, M. Valvo, and R. Younesi, *Mater. Today Energy*, **18**, 100505 (2020).
34. Nagmani and S. Puravankara, *ACS Appl. Energy Mater.*, **3**, 10045 (2020).
35. K. Kuratani, N. Uemura, H. Senoh, H. T. Takeshita, and T. Kiyobayashi, *J. Power Sources*, **223**, 175 (2013).
36. A. Ponrouch, R. Dedryvère, D. Monti, A. E. Demet, J. M. Ateba Mba, L. Croguennec, C. Masquelier, P. Johansson, and M. R. Palacín, *Energy Environ. Sci.*, **6**, 2361 (2013).
37. A. Fukunaga, T. Nohira, R. Hagiwara, K. Numata, E. Itani, S. Sakai, K. Nitta, and S. Inazawa, *J. Power Sources*, **246**, 387 (2014).
38. C. Ding, T. Nohira, R. Hagiwara, A. Fukunaga, S. Sakai, and K. Nitta, *Electrochim. Acta*, **176**, 344 (2015).
39. Q. W. Lin, J. Zhang, D. B. Kong, T. F. Cao, S.-W. Zhang, X. R. Chen, Y. Tao, W. Lv, F. Y. Kang, and Q. H. Yang, *Adv. Energy Mater.*, **9**, 1803078 (2019).